Current Biology 19, 1421–1428, September 15, 2009 ©2009 Elsevier Ltd All rights reserved DOI 10.1016/j.cub.2009.07.018

Article

Mechanosensing through Cooperative Interactions between Myosin II and the Actin Crosslinker Cortexillin I

Yixin Ren,[1] Janet C. Effler,[1,3,7] Melanie Norstrom,[5] Tianzhi Luo,[1] Richard A. Firtel,[6] Pablo A. Iglesias,[3] Ronald S. Rock,[5] and Douglas N. Robinson[1,2,4,*]
[1]Department of Cell Biology
[2]Department of Pharmacology and Molecular Sciences Johns Hopkins University School of Medicine, Baltimore, MD 21205, USA
[3]Department of Electrical and Computer Engineering
[4]Department of Chemical and Biomolecular Engineering Johns Hopkins University, Baltimore, MD 21218, USA
[5]Department of Biochemistry and Molecular Biology, University of Chicago, Chicago, IL 60637, USA
[6]Section of Cell & Developmental Biology, University of California, San Diego, La Jolla, CA 92093, USA

Summary

Background: Mechanosensing governs many processes from molecular to organismal levels, including during cytokinesis where it ensures successful and symmetrical cell division. Although many proteins are now known to be force sensitive, myosin motors with their ATPase activity and force-sensitive mechanical steps are well poised to facilitate cellular mechanosensing. For a myosin motor to experience tension, the actin filament must also be anchored.
Results: Here, we find a cooperative relationship between myosin II and the actin crosslinker cortexillin I where both proteins are essential for cellular mechanosensory responses. Although many functions of cortexillin I and myosin II are dispensable for cytokinesis, all are required for full mechanosensing. Our analysis demonstrates that this mechanosensor has three critical elements: the myosin motor where the lever arm acts as a force amplifier, a force-sensitive bipolar thick-filament assembly, and a long-lived actin crosslinker, which anchors the actin filament so that the motor may experience tension. We also demonstrate that a Rac small GTPase inhibits this mechanosensory module during interphase, allowing the module to be primarily active during cytokinesis.
Conclusions: Overall, myosin II and cortexillin I define a cellular-scale mechanosensor that controls cell shape during cytokinesis. This system is exquisitely tuned through the enzymatic properties of the myosin motor, its lever arm length, and bipolar thick-filament assembly dynamics. The system also requires cortexillin I to stably anchor the actin filament so that the myosin motor can experience tension. Through this cross-talk, myosin II and cortexillin I define a cellular-scale mechanosensor that monitors and corrects shape defects, ensuring symmetrical cell division.

Introduction

Similar to chemical cues that direct cell behaviors such as chemotaxis, cell proliferation, and cell fate specification, mechanical signals are important for guiding a range of physiological processes. At the organismal level, mechanosensing and mechanotransduction are at the core of many processes, including bone remodeling, hearing, muscle growth, and blood pressure regulation [1]. At the cellular level, mechanosensing is needed during processes like cytokinesis [2] and can help direct the differentiation of stem cells [3]. Molecularly, mechanosensing can occur through stretch-activated channels in the plasma membrane [4], through extension of focal adhesion-associated proteins (e.g., [5–7]), and potentially directly through myosin motors, which are force-transmitting enzymes [8–11]. Hearing adaptation likely occurs through a strain-sensitive myosin I family member, which adjusts its position on the actin filament to modulate the tension on the tip link, controlling channel opening [12]. In muscle, more myosin II motor domains (cross-bridges) are recruited into the load-bearing state when the muscle contracts under load than when it contracts without load (the Fenn effect; e.g., [13]). However, in nonmuscle cells, it is much less clear how myosins directly respond to cellular-scale mechanical loads because the myosin IIs are often in disorganized actin polymeric networks, rather than in paracrystalline arrays like those found in muscle. It is also unknown whether a single force-sensitive enzyme (myosin) is sufficient to mediate a cellular response or whether nonmuscle cellular mechanosensing is a function of an entire cytoskeletal network. Still, with its load-sensitive kinetic steps, nonmuscle myosin II is well poised to be at the center of a cellular-scale mechanosensor.

Previously, we discovered a mechanosensory system that helps govern cell shape progression during cytokinesis in *Dictyostelium* [2]. This mechanosensory system corrects natural shape defects during cell division by recruiting myosin II and the actin crosslinker cortexillin I to the site of cell deformation (hereafter referred to as the mechanosensory response). By using micropipette aspiration, we could control where the deformation occurred and direct myosin II and cortexillin I anywhere we wanted along the cortex (Figures 1A and 1B). Myosin II is essential for the shape control system and without it, the cells have altered cleavage furrow morphology, produce many more asymmetrically sized daughter cells, and cannot withstand mechanical perturbations. This shape control system does not depend on the mitotic spindle but is specific to cells in anaphase through the end of cytokinesis; interphase and early mitotic wild-type cells do not show myosin II or cortexillin I redistribution in response to these mechanical perturbations induced with physiologically relevant pressures.

Here, we demonstrate that myosin II and cortexillin I interact to form a cellular-scale mechanosensor. Unlike cytokinesis, which can be rescued with mutant forms of myosin II and cortexillin I, our results show that the mechanosensory system is an exquisitely tuned molecular system that requires fully wild-type myosin II and cortexillin I function. We show that myosin II thick-filament assembly and disassembly dynamics are required for the mechanosensory response, and that the small GTPase RacE is the cell-cycle-stage specificity factor. By using motor and lever arm mutants of myosin II, we demonstrate that the lever arm length specifies the pressure-threshold dependency of the responses. Finally, to generate

*Correspondence: dnr@jhmi.edu
[7]Present address: Human Genome Sciences, Inc., 14200 Shady Grove Road, Rockville, MD 20850, USA

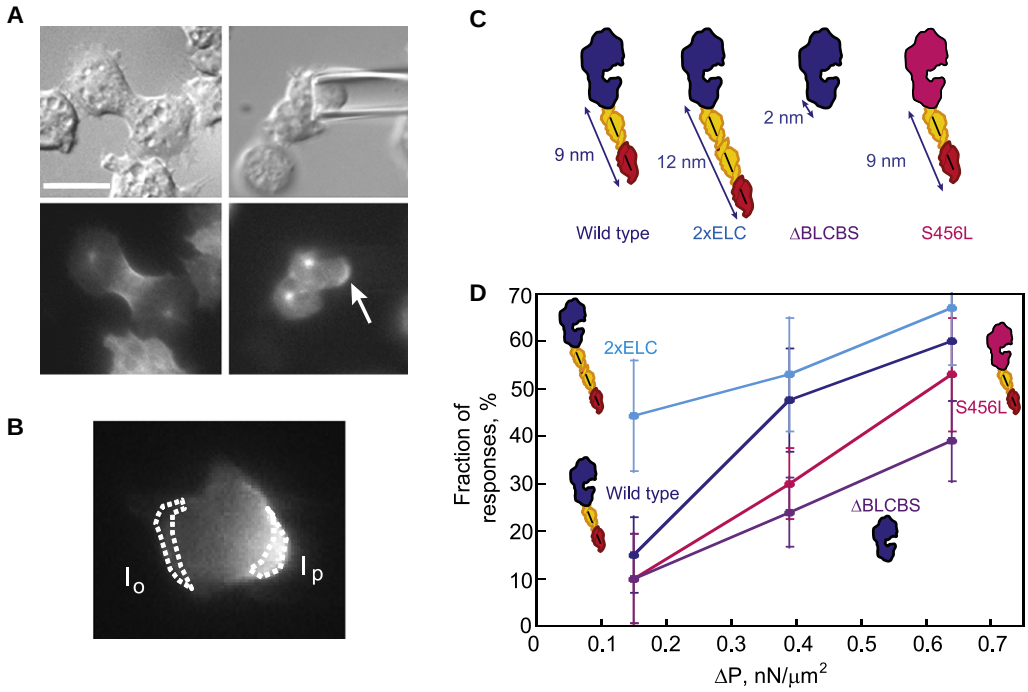

Figure 1. Myosin II Lever Arm Length Determines the Pressure-Threshold-Dependent Behavior of the Cellular Mechanosensory Response

(A) Representative micrographs showing a positive response to applied pressure. The cell is a *myoII*: Cit-ΔBLCBS;GFP-tubulin. Top panels, DIC images. Lower panels, fluorescence images. Left panels, cell before aspiration; right panels, cell during aspiration. The centrosomes are visible and Cit-ΔBLCBS accumulates at the micropipette (arrow). This cell is one of the positive responses of ΔBLCBS at 0.39 nN/μm^2 pressure. Scale bar represents 10 μm.

(B) Micrograph of a mitotic cell expressing wild-type GFP-myosin II, showing a response. The intensity of the cortex inside the micropipette (I_p) and the opposite cortex (I_o) were measured. The I_p/I_o ratio was calculated and the log transform was used for analysis.

(C) Cartoon comparing wild-type, 2xELC, ΔBLCBS, and S456L motors. Blue/pink, motor domain; yellow, essential light chain; red, regulatory light chain.

(D) Graph shows the dependency of the fraction of responses on the applied pressure. Here, the error bars are standard errors where SE = $\sqrt{(f(1-f)/n)}$, where f is the fraction of responses and n is the sample size. Frequency histograms of each data set and a second graph showing the overall average magnitudes (±SEMs) are provided in Figure S3 (see Experimental Procedures also). At 0.15 nN/μm^2 pressure, 2xELC is more responsive than wild-type, S456L, or ΔBLCBS myosins (Student's t test: $p < 0.01$). Wild-type and 2xELC myosin II are more responsive than ΔBLCBS at 0.39 and 0.64 nN/μm^2 pressure (Student's t test: $p < 0.01$).

tension, the myosin II must pull against stably anchored actin filaments. By using single-molecule methods, we demonstrate that cortexillin I dwells on the actin filaments on time scales much longer than the myosin, providing the stable anchoring required for mechanosensing. Overall, these data demonstrate that myosin II and cortexillin I cooperate to mediate cellular-scale mechanosensing during cell division.

Results

Wild-Type Myosin II Thick-Filament Assembly Dynamics, Regulatory Phosphorylation, and Mechanochemistry Are Required for the Mechanosensory Response

To determine how the mechanosensory system operates, we began with a complete structure-function analysis of myosin II. First, we examined the role of bipolar thick-filament (BTF) assembly dynamics in the mechanosensory response by analyzing cells expressing the nonphosphorylatable myosin II heavy chain mutant (the 3xAla mutant), which stably assembles into thick filaments, and the constitutively disassembled myosin II heavy chain mutant (the 3xAsp mutant). We anticipated that without assembling into BTFs [14, 15], 3xAsp myosin II would not accumulate at the micropipette, which proved to be the case (n = 10) (Figures S1A and S2, Table S1 available online). 3xAla myosin II overaccumulates at the cleavage furrow cortex during cytokinesis [14, 15]. However, in all cases, *myoII*: 3xAla; RFP-tub cells aspirated with a range of pressures (Δp = 0.22–0.79 nN/μm^2; n = 16) failed to accumulate 3xAla myosin II at the micropipette (Figures S1B and S2). Similarly, the minimal domain (assembly domain; GFP-RLC binding site-assembly domain [GRA]) that is necessary and sufficient for targeting myosin II to the cleavage furrow cortex but that lacks the BTF assembly regulatory region did not accumulate at the micropipette (Δp = 0.31–0.51 nN/μm^2; n = 6) (Figures S1C and S2; Table S1). Given that the assembly domain constitutively assembles into BTFs [16, 17], this result is analogous to the 3xAla result. These results indicate that the full thick-filament assembly and disassembly dynamics are essential for the mechanosensory system.

We then tested whether regulatory light chain (RLC) phosphorylation, which increases motor activity, is required for the mechanosensory response. In *Dictyostelium* cells, RLC phosphorylation is not required for cytokinesis, presumably because RLC phosphorylation activates the myosin II actin-activated ATPase activity only ~3- to 5-fold [18]. In addition, a 5-fold slower myosin II because of shortening of the lever arm (ΔBLCBS, a deletion of both light chain binding sites) [19] and a 10-fold slower myosin II (S456L) rescued cytokinesis dynamics [20]. Therefore, myosin II mechanochemistry is not rate limiting for cytokinesis over at least a 10-fold range of (unloaded) velocity. However, RLC phosphorylation was required for the mechanosensory response. Only 11% (n = 19) of *ΔRLC*

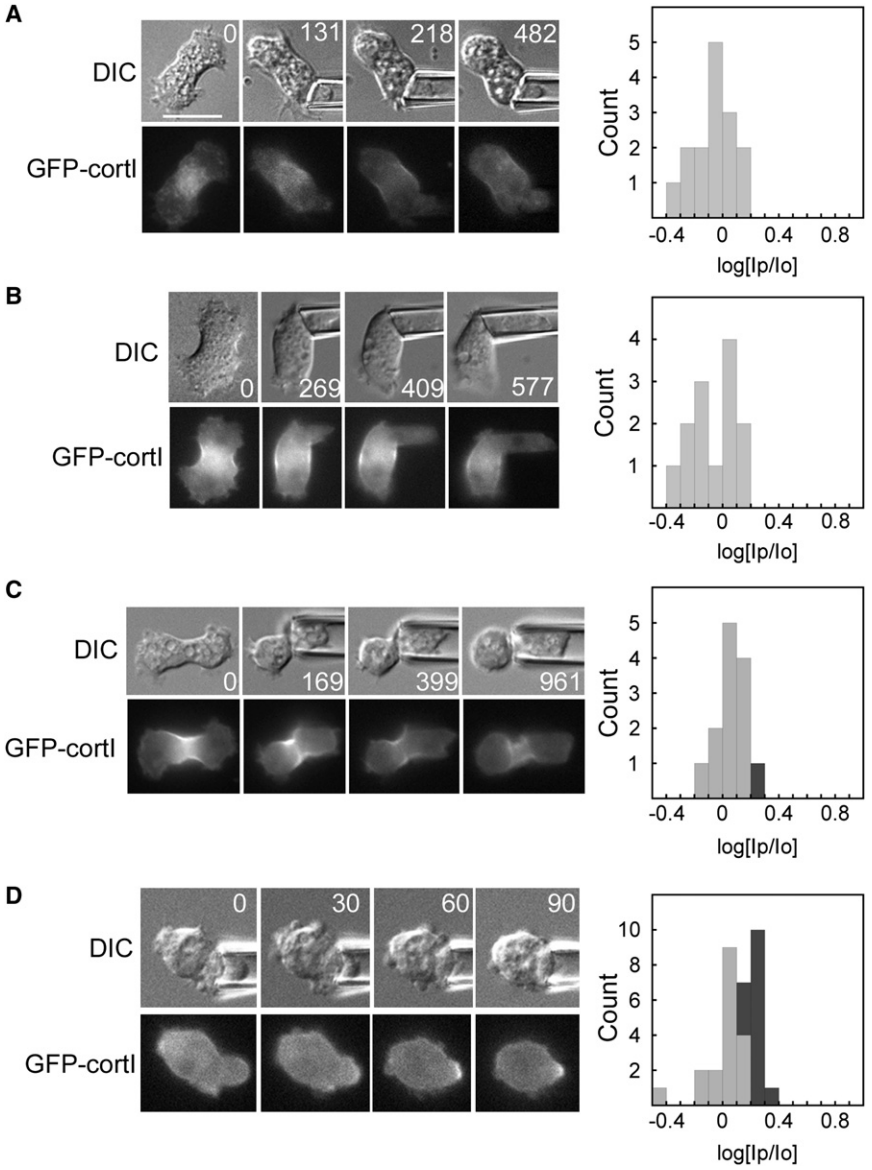

Figure 2. The Mechanosensitive Localization of Cortexillin I Requires Myosin II

Example time series (times in seconds) of DIC and fluorescent images are shown for (A) a *myoII*:GFP-cortI cell aspirated with 0.30 nN/μm^2 of pressure; (B) a *myoII*:GFP-cortI;dynhp cell aspirated with 0.21–0.28 nN/μm^2 of pressure; (C) a *myoII*:GFP-cortI;S456L cell aspirated with 0.26 nN/μm^2 of pressure; and (D) a *myoII*:GFP-cortI; myosin (rescue) cell aspirated with 0.45 nN/μm^2 of pressure. Frequency histograms show measurements from all cells measured for each genotype. As described in the Experimental Procedures, the dark gray bars of the histograms indicate positive responses, whereas light gray bars indicate negative responses. Statistical analysis indicated that the *myoII*:GFP-cortI and *myoII*:GFP-cortI;myoII strains are statistically distinct (Student's t test: $p < 0.001$). Scale bar represents 10 μm.

cells complemented with RLC S13A (a mutant RLC where the phosphorylation site has been mutated to alanine) showed any detectable response (Figures S1D and S2). In contrast, 64% of control cells (*ΔRLC* cells complemented with a wild-type RLC) responded to mechanical perturbation (n = 11; Table S1). Thus, full activation of the myosin II motor domain through regulatory light chain phosphorylation is required for full mechanosensing ability.

Myosin II Lever Arm Tunes the Pressure-Threshold Dependency

The results so far indicated that the motor activity itself is a critical component of the ability of the cells to mechanosense and suggested that myosin mechanochemistry could be the direct sensor. Myosin load dependency is commonly studied via single-molecule assays where either the motor or actin filament is anchored, and the other component is pulled on with an optical tweezer [8–11]. However, in our experimental setup, we use micropipette aspiration to pull on the cell cortex, which is a network of crosslinked actin polymers with embedded myosin II thick filaments [20]. We reasoned that we should be able to shift the pressure dependency of the mechanosensory response by altering lever arm length if myosin II is the cellular-scale mechanosensor, the myosin II lever arm is a rigid cantilever, and the maximum force production (F_{max}) by the myosin motor is inversely related to lever arm length [21] (Figure 1C). To analyze the data, we used two strategies (Experimental Procedures): we measured a response rate where responses are defined as a magnitude greater than two standard deviations of the interphase mean (wild-type interphase cells do not show a response [see below] [2]; Figure 1D), and we analyzed the entire distribution of the response magnitudes (Figure S3). The combination of analysis strategies yielded a more complete picture of the lever arm dependency. First, we defined the pressure dependency for the accumulation of wild-type myosin II (9 nm lever arm and 3 μm/s unloaded velocity) to the micropipette (Figure 1D; Figure S3). We then studied two lever arm mutants: ΔBLCBS and 2xELC (Figures 1A, 1C, and 1D). ΔBLCBS (2 nm lever arm, 0.6 μm/s unloaded velocity), which has a much higher predicted F_{max}, required greater applied pressure in order to respond (Figure 1D; Figure S3). Within the dynamic pressure range available for these experiments, the ΔBLCBS mutant myosin II did not respond to wild-type levels. In contrast, 2xELC (13 nm lever arm, 4 μm/s unloaded velocity), which is predicted to have a lower F_{max}, required much lower pressures to achieve wild-type levels of response (Figure 1D; Figure S3). Finally, because the unloaded velocities of the three lever arm lengths might explain the differences in responsiveness, we tested the 10- to 15-fold slower S456L myosin II (9 nm lever arm, 0.2 μm/s unloaded velocity), which has a wild-type lever arm [22]. The S456L myosin II showed a pressure dependency that was lower than wild-type myosin II at intermediate pressures, but then at high pressures, S456L myosin II responded nearly at wild-type levels and at higher levels than ΔBLCBS did

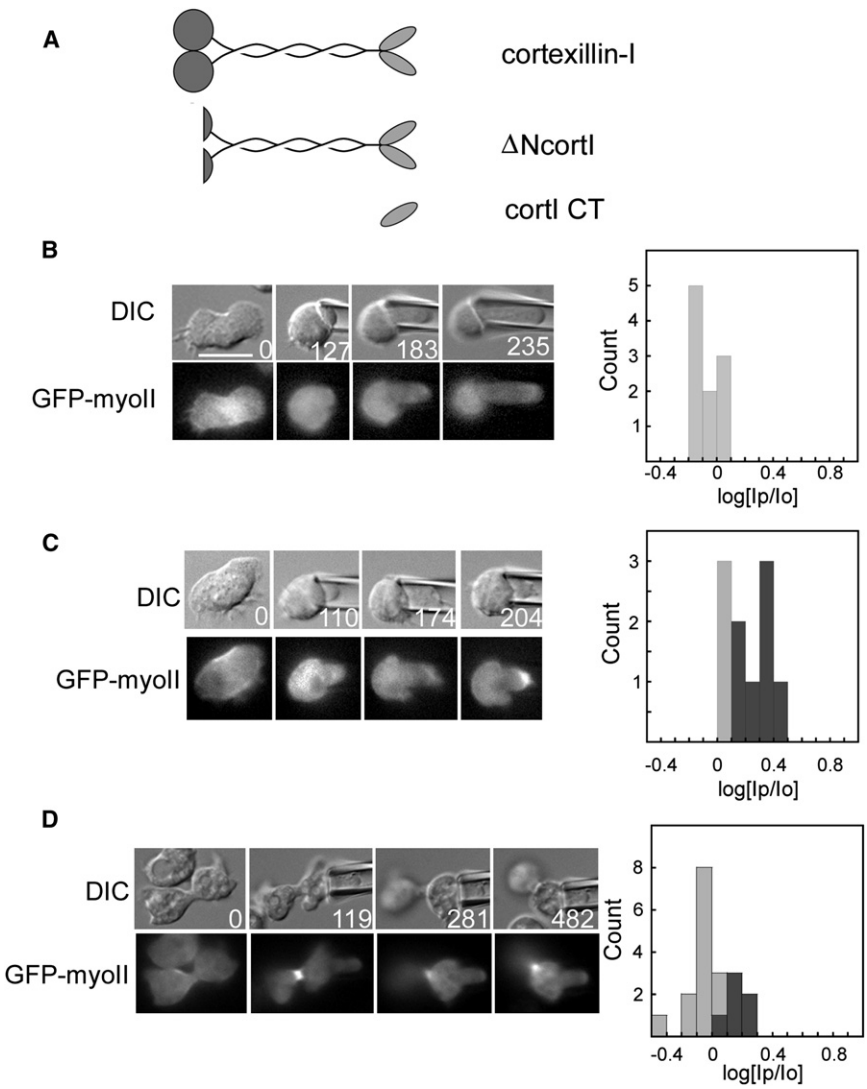

Figure 3. The Mechanosensitive Localization of Myosin II Requires Cortexillin I

(A) Wild-type cortexillin I, ΔNcortI, and cortI CT were tested for their ability to restore mechanosensory responses. All three proteins rescue cytokinesis [24, 25].

(B–D) Example time series (times in seconds) of DIC and fluorescence images are shown for (B) a *cortI*:GFP-myoII cell; (C) a *cortI*: GFP-myoII; RFP-cortI (full-length cortexillin I) cell; and (D) a *cortI*: GFP-myoII;RFP-ΔNcortI cell. Frequency histograms show measurements from all cells measured for each genotype. Statistical analysis indicated that the *cortI*: GFP-myoII;RFP-tub and *cortI*: GFP-myoII;RFP-cortI strains are statistically distinct (Student's t test: $p < 0.0001$). Scale bar represents 10 μm.

(Figure 1D; Figure S3). Thus, the unloaded velocity of myosin II is not the major determinant; rather the lever arm length tunes the pressure range over which the cell responds to applied mechanical strain. The simplest explanation is that the mechanical stress stabilizes the myosin II motor in the strongly bound state (increasing the duty ratio), and the lever arm length specifies the pressure required to lock the myosin II motor onto the actin. Because the slopes of each of the pressure curves are similar between the myosin motor and lever arm mutants, this observation suggests that it is a pressure threshold that triggers the response and the force amplification by the lever arm tunes where this threshold sits.

Cooperative Interactions between Myosin II and Cortexillin I Are Required for the Mechanosensory System

Because myosin II and cortexillin I are recruited to the micropipette [2], we then asked whether these proteins depend on each other for recruitment. In a *myoII* null background, cortexillin I did not localize in response to mechanical load (Δp = 0.15–0.43 nN/μm^2; n = 15) (Figure 2A). One hypothesis was that myosin II may help mobilize the crosslinked actin network, promoting cortexillin I mobility. To partially phenocopy this condition [23], we silenced expression of the actin crosslinker *dynacortin* by using RNAi in a *myoII*:GFP-cortI cell (Figure 2B). Cortexillin I recruitment to the pipette was not restored in *dynacortin* RNAi cells (Δp = 0.13–0.45 nN/μm^2; n = 13). Consistent with its lower mechanosensitivity particularly at lower pressures, S456L myosin II only partially rescued GFP-cortI recruitment to the micropipette (Δp = 0.24–0.87 nN/μm^2; n = 13) (Figure 2C). However, expression of unlabeled wild-type myosin II in a *myoII*: GFP-cortI background restored GFP-cortexillin I recruitment in 44% of the cells (Δp = 0.22–0.57 nN/μm^2; n = 32) (Figure 2D).

We then asked whether myosin II depends on wild-type cortexillin I (Figure 3A). In two different *cortexillin-I* null strains, GFP-myosin II did not move to the micropipette (Figure 3B; Table S1). However, this defect could be rescued to wild-type levels only with full-length cortexillin I (70% of cells responding, n = 10) (Figure 3C; Table S1). Previous structure-function studies indicated that only the carboxy-terminal domain of cortexillin I (cortI CT) is needed for cytokinesis, for PIP_2 binding and for actin crosslinking in vitro [24] (Figure 3A). We tested whether cortI CT (Table S1) and ΔN-cortextillin I (ΔNcortI), which is missing the amino-terminal calponin-homology domain that provides an additional actin-binding site, are sufficient for mechanosensing. CortI CT failed to rescue mechanosensing, and ΔNcortI rescued only to intermediate levels (Figure 3D; Table S1). Thus, as with myosin II, wild-type cortexillin I activity is required for mechanosensing. Because cortexillin I is an actin crosslinking protein, we tested whether this dependency on cortexillin I is a phenomenon general to any actin crosslinking protein. We analyzed mechanosensory responses in cells devoid of the actin crosslinkers dynacortin, enlazin, and fimbrin. None of these proteins was required for the mechanosensory response (Figure S4), which is consistent with the observation that they do not move to the micropipette as myosin II and cortexillin I do [2]. Overall, cortexillin I and myosin II depend on each other for accumulating in response to mechanical perturbation as part of the mechanosensory shape control pathway.

Myosins have load-sensitive actin-binding properties; yet for myosin to experience these loads, the actin filaments

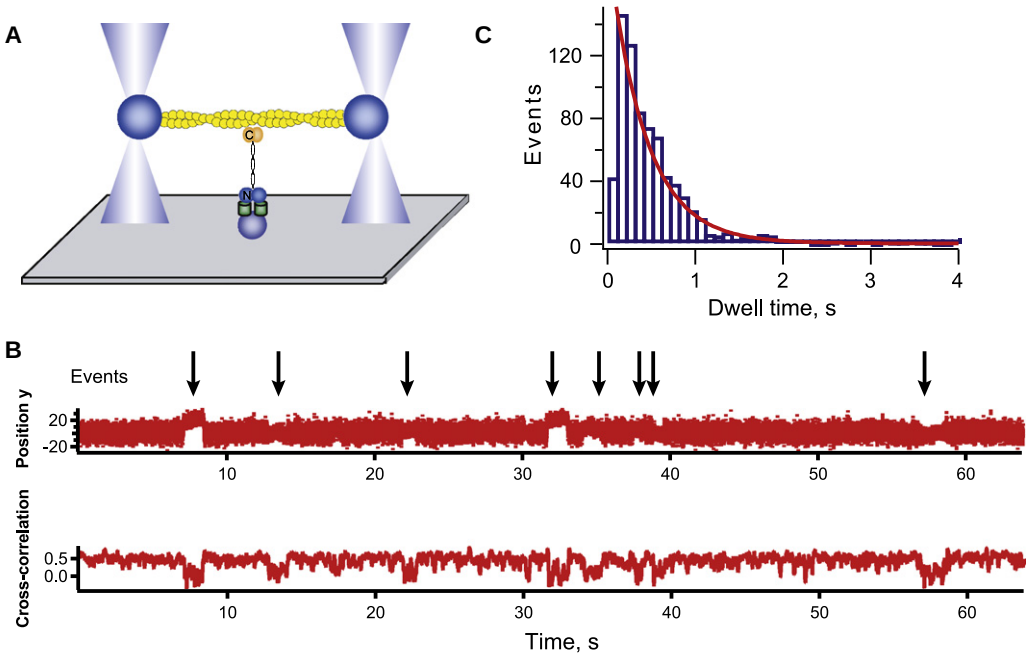

Figure 4. Single-Molecule Analysis of Cortexillin I-Actin Interactions

(A) Cartoon depicts the geometry of the experimental set up. GFP-cortexillin I is anchored to the substrate through the GFP via GFP antibodies. An actin dumbbell is steered into position by means of a dual beam optical trap.

(B) An example trace showing the bead position (top) and the cross-correlation of the fluctuations of the two beads (bottom) holding the actin dumbbell.

(C) Dwell time distribution showing the distribution of bound lifetimes. The mean τ is 550 ms (±40 ms, n = 776 events). Errors are standard errors from fitting bootstrap-sampled data sets.

must be anchored to the actin network or to the plasma membrane. These anchor points must be longer lived than the myosin motor-actin interaction. Unloaded *Dictyostelium* myosin II strongly bound state time is 2.4 ms [22], which may increase 10-fold to 24 ms under load (Supplemental Data). Because cortexillin I is essential for the mechanosensory response, we tested whether it remains bound to the actin for longer time scales than the myosin motor domain does. Previous FRAP studies indicated that cortexillin I turns over on the 5 s time scale [20]. However, in vivo FRAP may reflect multiple protein interactions. Therefore, we used a single-molecule approach to directly test the lifetime of a single cortexillin I-actin interaction (Figure 4A). We purified GFP-cortexillin I and measured the cortexillin I-actin dwell-time distribution (Figures 4B and 4C). We found that cortexillin I bound a single actin filament with an average dwell time (τ) of 550 ms, which is up to 200-fold longer than the myosin motor-actin strongly bound state time.

RacE Is the Cell-Cycle Stage Specificity Factor

Previously, we showed that without extreme deformation, this mechanosensory pathway was not active in wild-type cells during interphase [2]. Because RacE presides over a pathway of global actin crosslinking proteins—dynacortin, enlazin, and fimbrin—that control (resist) contractility dynamics during cytokinesis [20, 25, 26], we hypothesized that it might inhibit the mechanosensory pathway. We first confirmed that mitotic *RacE* mutant cells were mechanosensory. Indeed, *RacE* null cells accumulated GFP-myosin II at the micropipette during cytokinesis (40% responses; n = 5) (Figure 5A). However, during interphase, 62% (n = 37) of *RacE* null cells responded by accumulating GFP-myosin II (Figure 5B) and 41% (n = 37) responded by accumulating GFP-cortexillin I (Figure 5C) at the micropipette. This effect was reversed (rescued) by expressing mCherry-RacE in these *RacE* null cells (10%; 2 out of 20 cells responded) (Figure 5D). Thus, in wild-type cells, RacE shields this mechanosensory system during interphase (see Discussion).

Discussion

A feedback control system requires a sensor and a transducer. In the shape control system described here (Figure 6), the cell responds to mechanical perturbations in order to correct the shape defect so that high-fidelity (successful and symmetrical) cytokinesis may proceed. Myosin II and cortexillin I work as an ensemble to sense and respond to mechanical perturbation. Myosin II is uniquely poised to be a sensor and a transducer because it naturally has load-dependent actin-binding steps. Limited by the energy available from ATP hydrolysis, myosins must respond to applied forces either by holding on to the actin filament (myosin I and myosin II), by back stepping (myosin V), or by releasing from the actin track altogether [27]. However, for such a mechanism to operate, the actin filament itself must be anchored to the network in order for the myosin to generate enough tension to stall so that it dwells on the actin polymer. In this cytokinesis mechanosensory shape control system, cortexillin I appears to be a key actin crosslinker that works in concert with myosin II to respond to applied cellular deformation. Therefore, this study reveals that a cellular-scale mechanosensor requires three critical elements: the myosin motor domain with its active force transducer (myosin ATPase) and force amplifier (myosin lever arm), a force-sensitive element that allows myosin thick-filament accumulation, and an actin crosslinker (cortexillin I in this case) that stabilizes the actin filament so that tension may be generated (and therefore

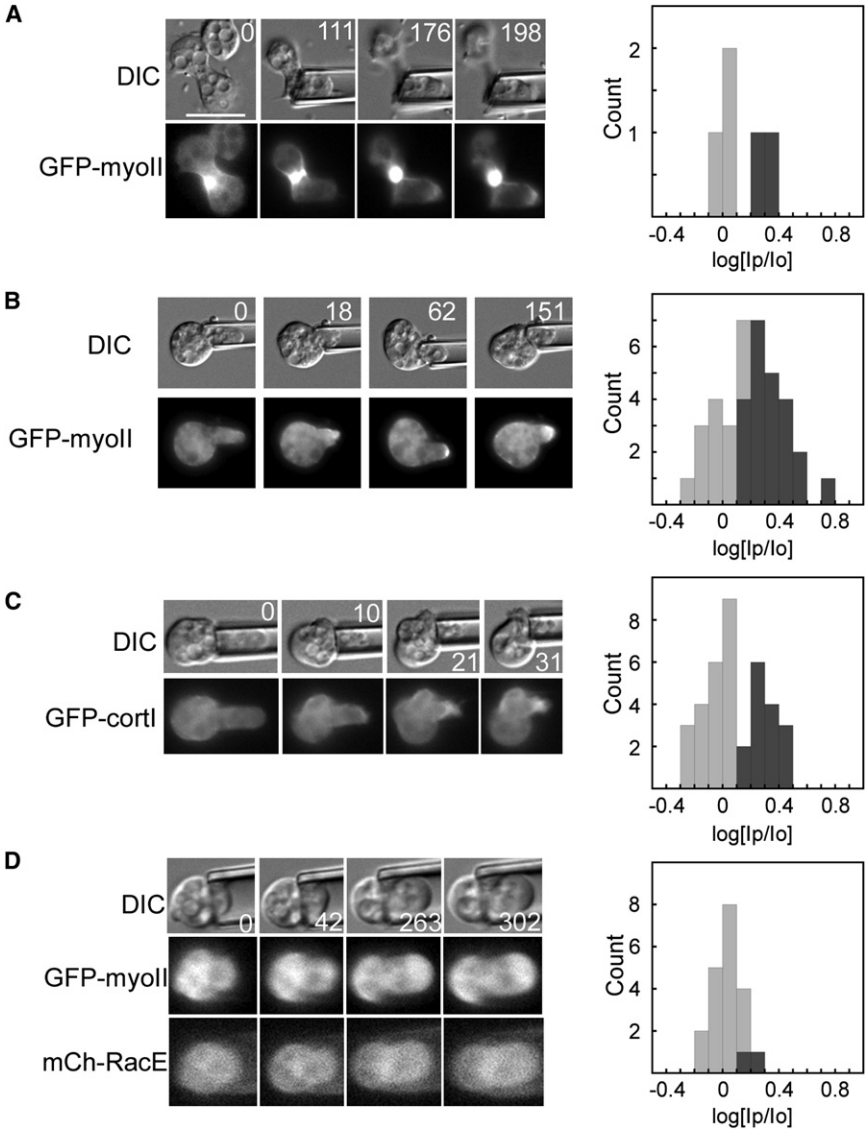

Figure 5. RacE Is the Cell-Cycle Stage Specificity Factor that Determines when Myosin II and Cortexillin I Can Redistribute in Response to Mechanical Strain

Example time series (times in s) of DIC and fluorescence images are shown for (A) a mitotic *RacE*: GFP-myoII cell; (B) an interphase *RacE*: GFP-myoII cell; (C) an interphase *RacE*: GFP-cortI cell; and (D) an interphase *RacE*: mCh-RacE;GFP-myoII cell. Frequency histograms show measurements from all cells measured for each genotype. Scale bar represents 10 μm.

experienced) by the motor domain as it goes through its power stroke (Figure 6A).

The lever arm tunes the pressure-threshold dependency of the response. From recent single-molecule studies, myosin I and myosin II move through substeps with different load sensitivities as they translocate along the actin filament [9, 11]. Complete transition through the substeps is required for ADP to be released, allowing ATP to bind so that the motor can release from the track. By varying the lever arm length, we were able to tune the pressure-threshold dependency of the cell's response. Similar to the single-molecule assays, our observations suggest that the mechanical stress that we apply to the cortex leads to strain on the myosin lever arm, preventing the motor from undergoing its full working stroke and locking the motor onto the filament for a longer period of time. Because of the longer lever arm (assuming the lever arm is a rigid rod and $F_{max} \propto$ [lever arm length]$^{-1}$; [21]), 2xELC (est. F_{max} = 2 pN) should require lower overall forces to strain the lever arm than the wild-type motor (F_{max} = 3 pN; [21]); consistently, it required less pressure to accumulate at the micropipette. In contrast, the short lever arm mutant ΔBLCBS (est. F_{max} = 14 pN) was much less sensitive and did not reach full wild-type mechanosensory response levels within the available pressure range for these experiments. This is consistent with the idea that a shorter lever arm requires greater forces to stall the motor. Because of its very short unloaded strongly bound state time (τ_s), it has not been feasible to measure the load dependency of τ_s for *Dictyostelium* myosin II. However, by comparing the active radial stress that we attribute to the cleavage furrow cortex during furrow ingression [26], the concentration of myosin II at the furrow cortex [15], and the pressure dependency of the mechanical response (this paper), estimates indicate that myosin II may undergo a 5- to 10-fold increase in duty ratio under mechanical stress (Supplemental Data). This is within range of the 5- to 12-fold increase in duty ratio for other myosin IIs [8]. One alternative hypothesis is that 2xELC achieves greater mechanosensitivity because it has a higher actin-activated ATPase activity that is insensitive to RLC phosphorylation (i.e., 2xELC is an unregulated motor, which behaves more similarly to RLC-phosphorylated wild-type myosin II). However, we disfavor this possibility because ΔBLCBS is similarly unregulated [21] but is significantly less mechanosensitive. Another alternative hypothesis is that the mechanosensory responsiveness is simply due to differences in the unloaded velocities of the different motors (wild-type, 3 μm/s; 2xELC, 4 μm/s; and ΔBLCBS, 0.6 μm/s; [21]). However, we disfavor this hypothesis because the 10-fold slower S456L myosin-II (0.2 μm/s; [22]) was more responsive than the 5-fold slower ΔBLCBS mutant. S456L achieves its reduced unloaded velocity through a 3-fold longer ADP-bound state and a normal step size [22]. Although the S456L protein undoubtedly undergoes its complete conformational change, without load it likely releases prematurely, yielding a fractional productive step. Thus, our observations suggest that loading this motor restores its ability to lock onto the actin filaments. These observations are consistent with in vivo mechanical data on interphase and dividing cells [20]. During interphase, cells expressing S456L have mechanical properties intermediate between wild-type and *myoII* null cells. However, during cytokinesis, the S456L mutant fully restores cell mechanics and

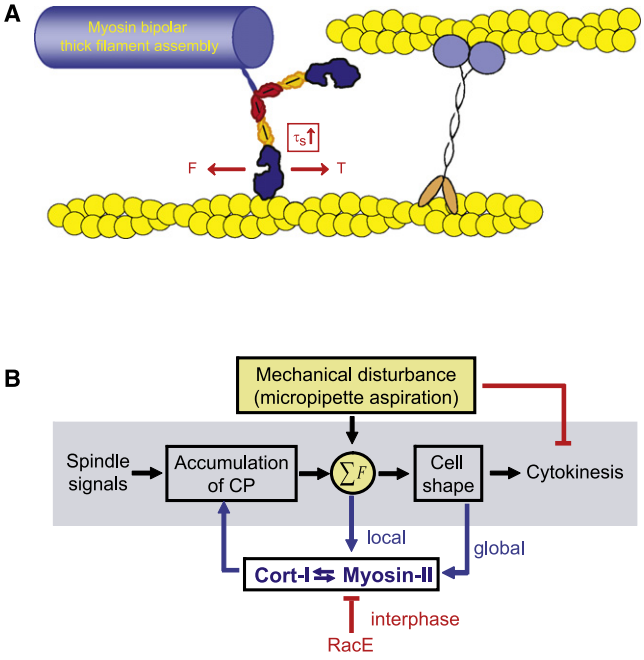

Figure 6. Mechanosensory Cell Shape Control System

(A) Cartoon depicts the mechanical circuit between myosin II and cortexillin I that mediates mechanosensing. Because tension is required to balance the myosin power stroke, which generates a force (F) on the actin filament, cortexillin I likely anchors the actin filament, providing the tension (T) needed to increase the strongly bound state time (τ_s). This cross-communication between myosin II and cortexillin I stabilizes each protein on the actin, promoting their accumulation. This stabilization also appears to provide feedback on myosin II thick filament assembly, allowing thick filaments to form, a requisite for accumulation.

(B) This mechanosensory system ensures successful high-fidelity cytokinesis. Mechanical perturbation halts cytokinesis during early stages of cytokinesis and triggers accumulation of myosin II and cortexillin I to the site of mechanical deformation during all stages of cytokinesis. Cooperative interactions between myosin II and cortexillin I define the cellular-scale mechanosensor.

cytokinesis furrow ingression dynamics to wild-type levels, suggesting that the mechanical stress in the dividing cell allows the S456L myosin II to function like a wild-type motor.

The mechanosensory system is likely to be highly cooperative. Based on our data, we find that elements of myosin mechanochemistry (full ATPase activity, regulatory light-chain phosphorylation, and lever arm) as well as bipolar thick filament assembly dynamics are required for the response. Thick-filament assembly requires a nucleation step and is delicately balanced by small electrostatic charge differences just downstream of the assembly domain [17, 28]. Our observations suggest that as mechanical stress locks the myosin II motor onto actin, it promotes the formation of bipolar thick filaments. Simulations indicate that a potential force-sensitive step could in fact be in the transition between assembly-incompetent and -competent states (Supplemental Data). Further, cortexillin I accumulates directly in a myosin II activity-dependent manner. Cortexillin I responds cotemporally with myosin II, S456L only partially restores cortexillin I recruitment consistent with S456L's weak activity, and cortexillin I accumulates in interphase *RacE* mutants similar to myosin II. We suggest that mechanical stress in the cortical actin network stabilizes myosin II and cortexillin I, allowing both to accumulate in a cooperative fashion.

This study has other important implications for both cellular mechanosensing and cell shape control. The global cortex has increased mechanical deformability during cytokinesis as compared to interphase [20], and we now find that the Rac-family small GTPase RacE determines the cell cycle specificity of the mechanosensory nature of the cortex (Figure 5B). This Rac acts as an inhibitor of cytokinesis contractility [26]. Because RacE is required for cortical tension and maintenance of other actin crosslinkers in the cortex ([20, 25] and references therein), RacE controls mechanical resistance. Given the fluid nature of *RacE* null cells [26], its presence in wild-type cells may make the cortex more elastic (solid-like) so that the mechanical stress is absorbed by the crosslinked network. During wild-type cell division (or in interphase *RacE* null cells), the cortical network becomes more deformable so that the myosin II/cortexillin I sensor now bears the mechanical stress, directing these proteins' accumulation at sites of shape deformation.

In addition to the shape control system, the cooperative interactions between myosin II and cortexillin I undoubtedly drive contractility at the cleavage furrow cortex. Null mutants in either gene have similarly altered cleavage furrow morphology, asymmetry in daughter cell sizes, and similar furrow ingression dynamics [2, 20, 26, 29]. The fact that neither protein requires the other for localization to the cleavage furrow cortex highlights that there are multiple pathways that direct their localization. Once myosin II and cortexillin accumulate at the furrow cortex, myosin II motors likely pull against cortexillin I, generating contractile stress in the actin network to help drive cleavage furrow constriction. In other scenarios, other crosslinkers or combinations of crosslinkers may also interact cooperatively with myosin II in a similar manner as cortexillin I does here.

In sum, this study reveals that myosin II mediates cellular-scale mechanosensing in nonmuscle cells to monitor and correct cell shape changes during cytokinesis. Because *Dictyostelium* are protozoans with numerous features similar to human cells, this mechanosensory system likely reflects an early requirement for cells to feel and respond to mechanical inputs from their environment and to monitor shape change progression during cell division. Myosin II may have evolved some of its mechanosensitive enzymatic steps in this context. Mechanosensitive myosin-dependent processes like hearing, muscle contraction, and cardiovascular function are undoubtedly late evolutionary beneficiaries of this cellular-scale mechanosensory module.

Experimental Procedures

Cell Strains

Dictyostelium discoideum strains and plasmids are described in full in the Supplemental Experimental Procedures and Table S1.

Micropipette Aspiration

Micropipette aspiration experiments were performed as previously described [2]. In short, micropipettes were pulled to an inner radius, ranging from 2 to 3 μm. With a motorized water manometer system, aspiration pressure was applied to the surface of the cell. To quantify responses, the fluorescent signal intensities (after background subtraction) of the cortex inside the pipette (I_p) and outside the pipette at the opposite cortex (I_o) were measured. Ratios of I_p/I_o greater than 1.39 ($\log(I_p/I_o) = 0.14$), which is two standard deviations above the wild-type interphase mean (as defined in [2]), were considered positive responses. In the frequency histograms, the positive responses are colored dark gray and negative responses are colored light gray. To determine standard errors for the fraction of responses (for Figure 1D), we used SE = $\sqrt{(f(1 - f)/n)}$, where f is the fraction

of responses and n is the sample size. We also analyzed the entire histograms for overall mean and standard errors for statistical testing (Student's t test). This approach does not require any additional assumptions about the responses, and we find that the use of both types of analyses provides a more complete picture of the data. Finally, particularly for the lever arm length and S456L mutants, we analyzed and compared the total signal intensities of the aspirated cells prior to aspiration to confirm that the exact cells analyzed had comparable (statistically identical) expression levels. Similar expression levels for each protein were generally the case across all of the strains studied.

Single-Molecule Analysis

His-tagged GFP-cortexillin I was expressed and purified to homogeneity from *E. coli* with polyethyleneimine and ammonium sulfate cuts followed by Ni^{2+}-NTA, size exclusion, and mono S column chromatography. The purified protein was tested in actin high-speed cosedimentation assays, confirming that it saturated actin with the expected 1 mole of cortexillin I dimer per 4 actins (data not shown) [30]. The GFP-cortexillin I was then anchored to a platform bead with anti-GFP monoclonal antibody (QBiogene, 3E6). Neutravidin-coated 1 μm biotinylated polystyrene beads (Molecular Probes) were attached to the ends of actin filaments assembled with 10% biotin-labeled actin monomers, creating actin dumbbells. An actin dumbbell was steered with a dual-beam optical trap by using acousto-optic modulators over individual platform beads in search of platforms that interacted with the actin filament. The positions of both beads of the actin dumbbell and their cross-correlation were monitored. Cortexillin I-actin interactions were determined by a decrease in the cross-correlated fluctuations of the two beads. Binding lifetimes were measured and plotted. The distributions largely fit a single exponential from which the cortexillin I-binding lifetime was determined. The probability that binding events were the result of two cortexillin molecules, instead of one, is ~4%. The buffer used for these assays contains 25 mM KCl, 25 mM imidazole•HCl (pH 7.5), 1 mM EGTA, 4 mM $MgCl_2$, 0.086 mg/mL glucose oxidase, 0.014 mg/mL catalase, 0.09 mg/mL glucose, and 1 mM DTT.

Supplemental Data

Supplemental Data include Supplemental Experimental Procedures, Supplemental Analysis, seven figures, and one table and can be found with this article online at http://www.cell.com/current-biology/supplemental/S0960-9822(09)01400-6.

Acknowledgments

We thank the *Dictyostelium* stock center for the RLC mutant strains and James Spudich for the 3xAla and 3xAsp constructs. We thank Sue Craig, Rob Jensen, and Carolyn Machamer for helpful comments on the manuscript. This work was supported by ACS grant RSG CCG-114122 (to D.N.R.), NIH grants GM066817 (to D.N.R.) and GM078450 (to R.S.R), and NSF grant CCF 0621740 (to P.A.I. and D.N.R.).

Received: May 12, 2009
Revised: July 2, 2009
Accepted: July 3, 2009
Published online: July 30, 2009

References

1. Orr, A.W., Helmke, B.P., Blackman, B.R., and Schwartz, M.A. (2006). Mechanisms of mechanotransduction. Dev. Cell *10*, 11–20.
2. Effler, J.C., Kee, Y.-S., Berk, J.M., Tran, M.N., Iglesias, P.A., and Robinson, D.N. (2006). Mitosis-specific mechanosensing and contractile protein redistribution control cell shape. Curr. Biol. *16*, 1962–1967.
3. Engler, A.J., Sen, S., Sweeney, H.L., and Discher, D.E. (2006). Matrix elasticity directs stem cell lineage specification. Cell *126*, 677–689.
4. Martinac, B. (2004). Mechanosensitive ion channels: Molecules of mechanotransduction. J. Cell Sci. *117*, 2449–2460.
5. Balaban, N.Q., Schwartz, U.S., Riveline, D., Goichberg, P., Tzur, G., Sabanay, I., Mahalu, D., Safran, S., Bershadsky, A.D., Addadi, L., and Geiger, B. (2001). Force and focal adhesion assembly: a close relationship studied using elastic micropatterned substrates. Nat. Cell Biol. *3*, 466–472.
6. Friedland, J.C., Lee, M.H., and Boettiger, D. (2009). Mechanically activated integrin switch controls a_5b_1 function. Science *323*, 642–644.
7. del Rio, A., Perez-Jimenez, R., Liu, R., Roca-Cusachs, P., Fernandez, J.M., and Sheetz, M.P. (2009). Stretching single talin rod molecules activates vinculin binding. Science *323*, 638–641.
8. Kovacs, M., Thirumurugan, K., Knight, P.J., and Sellers, J.R. (2007). Load-dependent mechanism of nonmuscle myosin 2. Proc. Natl. Acad. Sci. USA *104*, 9994–9999.
9. Veigel, C., Molloy, J.E., Schmitz, S., and Kendrick-Jones, J. (2003). Load-dependent kinetics of force production by smooth muscle myosin measured with optical tweezers. Nat. Cell Biol. *5*, 980–986.
10. Altman, D., Sweeney, H.L., and Spudich, J.A. (2004). The mechanism of myosin VI translocation and its load-induced anchoring. Cell *116*, 737–749.
11. Laakso, J.M., Lewis, J.H., Shuman, H., and Ostap, E.M. (2008). Myosin I can act as a molecular force sensor. Science *321*, 133–136.
12. Gillespie, P.G., and Cyr, J.L. (2004). Myosin-1c, the hair cell's adaptation motor. Annu. Rev. Physiol. *66*, 521–545.
13. Ford, L.E., Huxley, A.F., and Simmons, R.M. (1985). Tension transients during steady shortening of frog muscle fibres. J. Physiol. *361*, 131–150.
14. Sabry, J.H., Moores, S.L., Ryan, S., Zang, J.-H., and Spudich, J.A. (1997). Myosin heavy chain phosphorylation sites regulate myosin localization during cytokinesis in live cells. Mol. Biol. Cell *8*, 2647–2657.
15. Robinson, D.N., Cavet, G., Warrick, H.M., and Spudich, J.A. (2002). Quantitation of the distribution and flux of myosin-II during cytokinesis. BMC Cell Biol. *3*, 4.
16. Shu, S., Liu, X., and Korn, E.D. (2003). *Dictyostelium* and *Acanthamoeba* myosin II assembly domains go to the cleavage furrow of *Dictyostelium* myosin II-null cells. Proc. Natl. Acad. Sci. USA *100*, 6499–6504.
17. Hostetter, D., Rice, S., Dean, S., Altman, D., McMahon, P.M., Sutton, S., Tripathy, A., and Spudich, J.A. (2004). *Dictyostelium* myosin bipolar thick filament formation: Importance of charge and specific domains of the myosin rod. PLoS Biol. *2*, e356.
18. Chen, P., Ostrow, B.D., Tafuri, S.R., and Chisholm, R.L. (1994). Targeted disruption of the *Dictyostelium* RMLC gene produces cells defective in cytokinesis and development. J. Cell Biol. *127*, 1933–1944.
19. Zang, J.-H., Cavet, G., Sabry, J.H., Wagner, P., Moores, S.L., and Spudich, J.A. (1997). On the role of myosin-II in cytokinesis: Division of *Dictyostelium* cells under adhesive and nonadhesive conditions. Mol. Biol. Cell *8*, 2617–2629.
20. Reichl, E.M., Ren, Y., Morphew, M.K., Delannoy, M., Effler, J.C., Girard, K.D., Divi, S., Iglesias, P.A., Kuo, S.C., and Robinson, D.N. (2008). Interactions between myosin and actin crosslinkers control cytokinesis contractility dynamics and mechanics. Curr. Biol. *18*, 471–480.
21. Uyeda, T.Q., Abramson, P.D., and Spudich, J.A. (1996). The neck region of the myosin motor domain acts as a lever arm to generate movement. Proc. Natl. Acad. Sci. USA *93*, 4459–4464.
22. Murphy, C.T., Rock, R.S., and Spudich, J.A. (2001). A myosin II mutation uncouples ATPase activity from motility and shortens step size. Nat. Cell Biol. *3*, 311–315.
23. Girard, K.D., Kuo, S.C., and Robinson, D.N. (2006). *Dictyostelium* myosin-II mechanochemistry promotes active behavior of the cortex on long time-scales. Proc. Natl. Acad. Sci. USA *103*, 2103–2108.
24. Stock, A., Steinmetz, M.O., Janmey, P.A., Aebi, U., Gerisch, G., Kammerer, R.A., Weber, I., and Faix, J. (1999). Domain analysis of cortexillin I: actin-bundling, PIP_2-binding and the rescue of cytokinesis. EMBO J. *18*, 5274–5284.
25. Robinson, D.N., and Spudich, J.A. (2000). Dynacortin, a genetic link between equatorial contractility and global shape control discovered by library complementation of a *Dictyostelium discoideum* cytokinesis mutant. J. Cell Biol. *150*, 823–838.
26. Zhang, W., and Robinson, D.N. (2005). Balance of actively generated contractile and resistive forces controls cytokinesis dynamics. Proc. Natl. Acad. Sci. USA *102*, 7186–7191.
27. Kee, Y.-S., and Robinson, D.N. (2008). Motor proteins: Myosin mechanosensors. Curr. Biol. *18*, R860–R862.
28. Moores, S.L., and Spudich, J.A. (1998). Conditional loss-of-myosin-II-function mutants reveal a position in the tail that is critical for filament nucleation. Mol. Cell *1*, 1043–1050.
29. Girard, K.D., Chaney, C., Delannoy, M., Kuo, S.C., and Robinson, D.N. (2004). Dynacortin contributes to cortical viscoelasticity and helps define the shape changes of cytokinesis. EMBO J. *23*, 1536–1546.
30. Faix, J., Steinmetz, M., Boves, H., Kammerer, R.A., Lottspeich, F., Mintert, U., Murphy, J., Stock, A., Aebi, U., and Gerisch, G. (1996). Cortexillins, major determinants of cell shape and size, are actin-bundling proteins with a parallel coiled-coil tail. Cell *86*, 631–642.

Current Biology, Volume *19*

Supplemental Data

Mechanosensing through Cooperative Interactions between Myosin II and the Actin Crosslinker Cortexillin I

Yixin Ren, Janet C. Effler, Melanie Norstrom, Tianzhi Luo, Richard A. Firtel, Pablo A. Iglesias, Ronald S. Rock, and Douglas N. Robinson

SUPPLEMENTAL EXPERIMENTAL PROCEDURES

Cell Strains

Dictyostelium discoideum strains are presented in Table S1. Constructs were transformed into wild type strain (Ax2 or Ax3:Rep orf+; HS1000) [1], the myosin-II heavy chain null (*myoII*) strain (*mhcA*; HS1) [2], *ΔRLC*:RLCwt, *ΔRLC*:RLCS13A [3], *cortexillin-I* null strains (cortIRF and HS1151) [4], and *RacE*^{24EH6} null (and its parental DH1) strain [5] and selected in 1.4x HL5, containing 8% FM (Enriched HL-5) and 15-30 µg/ml G418, 4 µg/ml blasticidin, and/or 15-30 µg/ml hygromycin as appropriate. Actin crosslinkers dynacortin, enlazin, and fimbrin were silenced using RNAi, and knockdown was confirmed by western analysis (not shown) as described previously [6-8].

Tubulin was observed using pDXA-BI: RFP-α-tubulin or pDRH:GFP- or RFP-α-tubulin [9]. Myosin-II was observed by using GFP-myosin-II:pBIG [10], and GFP-3xAla:pBIG and GFP-3xAsp:pBIG constructs [11]. The citrine (enhanced YFP) fluorescent protein labeled myosin-II series was constructed in pDRH for this paper. The citrine cDNA was ligated into the *Bgl* II and *Sal* I sites in pDRH. A *Sac* I site was introduced in the myosin-II heavy chain cDNA at the end of the lever arm as defined in [12]. The myosin-II heavy chain tail was subcloned into the *Sal* I and *Not* I sites of pDRH, with the 5' primer carrying the *Sal* I and *Sac* I sites. The motor mutants were amplified using a 5' primer, which included an in-frame *Sal* I site, and a 3' primer, which included the in-frame *Sac* I site. The two lever arm mutants (2xELCBS and ΔBLCBS) were constructed as defined in [12]. The GRA myosin fragment includes a GFP fused to the regulatory light chain binding site, which is then linked to the assembly domain [13, 14].

The RFP-cortexillin full-length, RFP-ΔNcortI, RFP-cortI CT, and mCherry-RacE expression plasmids were constructed by first generating RFP- and mCherry-tagging cassettes in pBlueScript, similar to our GFP-tagging system described previously [4, 9]. Once each cDNA was cloned into the respective tagging cassette, the fluorescent protein-fusion cDNAs were subcloned into pDRH for expression in *Dictyostelium*.

SUPPLEMENTARY ANALYSIS

The mechanosensory system involves three apparent elements: load-sensitive motor domain-actin interactions, cortexillin-I-actin anchoring, and myosin-II thick filament assembly dynamics. Here, we deal with the load-sensitivity of the motor domain and the myosin-II thick filament assembly dynamics.

Load sensitivity of the motor domain

From the concentration at the cleavage furrow cortex during cytokinesis, myosin-II reaches concentrations of 5-6 μM and furrow cortex:polar cortex ratios of ~1.6-2. These ratios were originally measured using ratio imaging with volumetric indicators [15]. However, because the myosin-II concentrates along the lateral edges of the cortex, the volumetric normalization offers only a nominal correction [8]. We assessed the concentration ratio of furrow to polar cortex, which agrees directly with the ratio from the volume-corrected analysis (Fig. S5).

With 5-6 μM myosin-II concentration and the volume of the cortex under the micropipette (Fig. S6), this corresponds to 40,000 myosin hexameric monomers (M; each with two motor heads) in the bipolar thick filament (BTF) form in the cortex. We estimate the active surface stress from myosin-II where the myosin-II-generated surface stress (σ) is

$$\sigma = \frac{\text{n heads in BTF form x duty ratio x F/head}}{\text{SA}}$$

where F is the force generated by a myosin head (3 pN), duty ratio is the fraction of myosin heads in the force-generating state as compared to the total number of available heads (assumed to be in the BTF assembled state and is 0.6% for unloaded *Dictyostelium* myosin-II), and SA is the surface area of the cortex under the micropipette. From this, we calculate σ to be 0.04 nN/μm^2, which agrees with the active radial stresses at the cleavage furrow (0.04-0.1 nN/μm^2) determined previously [16]. However, for accumulation of myosin-II to the micropipette, 0.4-0.6 nN/μm^2 pressure was required. If the myosin-II heads are recruited into the load-bearing state to directly off-set the applied pressure, then the myosin-II could reasonably undergo a 5-10-fold shift in duty ratio (0.4 nN/μm^2/0.04 nN/μm^2), which compares well with the load-dependent shifts in duty ratio observed for other myosin-II enzymes [17, 18].

Myosin-II thick filament assembly

Our data indicate that myosin-II must be able to undergo full assembly-disassembly in order to accumulate during the mechanosensory response. These observations suggest that there is likely to be a mechanosensitive step during thick filament assembly. The assembly pathway and the kinetic parameters are largely known.

$$
\begin{aligned}
M_0 &\underset{k_{-1}}{\overset{k_1}{\rightleftharpoons}} M, & k_1 &= 0.0008\,\mathrm{s}^{-1} \\
& & k_{-1} &= 0.1\,\mathrm{s}^{-1} \\
M + M &\underset{k_{-2}}{\overset{k_2}{\rightleftharpoons}} D, & k_2 &= 0.37\,\mu\mathrm{M}^{-1}\mathrm{s}^{-1} \\
& & k_{-2} &= 0.01\,\mathrm{s}^{-1} \\
D + D &\underset{k_{-3}}{\overset{k_3}{\rightleftharpoons}} T, & k_3 &= 0.0395\,\mu\mathrm{M}^{-1}\mathrm{s}^{-1} \\
& & k_{-3} &= 0.0045\,\mathrm{s}^{-1} \\
T + D &\underset{k_{-4}}{\overset{k_4}{\rightleftharpoons}} BTF_3, & k_4 &= 1.25\,\mu\mathrm{M}^{-1}\mathrm{s}^{-1} \\
& & k_{-4} &= 0.025\,\mathrm{s}^{-1} \\
BTF_n + D &\underset{k_{-5}}{\overset{k_5}{\rightleftharpoons}} BTF_{n+1}, & k_5 &= 10\,\mu\mathrm{M}^{-1}\mathrm{s}^{-1} \\
& & k_{-5} &= 0.2\,\mathrm{s}^{-1}
\end{aligned}
$$

M_0 is the assembly incompetent (stabilized in part by heavy chain phosphorylation) hexameric monomer, M is the assembly-competent monomer, D is the parallel dimer, T is anti-parallel tetramer, which is thought to be the first stable nucleus, and BTF_n is the bipolar thick filament with n dimers. We consider BTFs that include 3 to 36 dimers. The rates for conversion between M_0 and M were chosen so that, at steady state, M_0 accounts for approximately 80% of total myosin [19]. Rates for k_2, k_{-2}, k_3, k_{-3}, k_4 and k_{-4} are derived from [20, 21]. The value of k_{-5} is derived from fluorescence recovery after photobleaching analysis [8, 22]. We also make the assumption that every time a dimer is added or released, the probability of further addition/removal is the same. Simulations based on this model were used to determine where the system is most sensitive. First, we allowed the myosin BTFs to assemble until steady state was reached. Then, to determine where force generation can have an appreciable effect on BTF concentration, we perturbed all 10 kinetic parameters in the model 10-fold, which was the amount estimated from the potential shift in duty ratio and strongly bound state time estimated above. The greatest effect was found to be in the rates between M and M_0. A ten-fold decrease in k_{-1} resulted in a ~50% increase in myosin found in the BTF after 60 s (Fig. S7). To mimic the 3xAla mutants, we also eliminated the assembly incompetent hexamer, M_0. In this case, the effect of changing other parameters was negligible, because at this point, nearly all the myosin is already in BTF form. Finally, we present the time-course for simulated assembly, which occurred on the minute time-scale, and the distribution of sizes of BTFs at 60 s compared to the initial steady state.

Three conclusions may be drawn from this analysis. First, the largest impact on the assembly dynamics comes from changing the rates of converting M_0 to M. This could occur because myosin motor binding to actin polymers is highly cooperative. By stabilizing motor domains on the actin this may allow free M to bind the actin placing them in close proximity for assembly into BTFs. It is notable that at steady state, our simulations indicate that most of the thick filaments do not reach the full 72 mer size [20]. Rather they populate a distribution of intermediate sizes of BTFs, which is similar to previous simulations of the assembly of muscle

myosin thick filaments [23]. Therefore, it is likely that when new M binds the actin polymers they directly insert into pre-existing BTFs. Moreover, the addition of actin polymers to myosin-II BTF assembly reactions *in vitro* eliminates the lag-phase characteristic of the nucleation phase [20]. This observation has interesting implications for myosin-II recruitment in other scenarios as well. For example, myosin-II may typically exist as a mixture of intermediate BTF sizes so that when signals trigger accumulation, the free monomers just have to incorporate directly into the BTFs. Myosin heavy chain phosphorylation then would ensure that the system relaxes back to the initial steady state distribution after the accumulation signal terminates. Second, these simulations demonstrate that 3xAla myosin-II would not respond to mechanical stress because there is insufficient available free M to respond. Third, these simulations offer one explanation why myosin-II accumulation in response to mechanical load requires one to a couple of minutes; the kinetic parameters for myosin BTF assembly are set to require that amount of time for accumulation. However, it is important to bear in mind that this analysis is not intended to be a full treatment of the system as it clearly does not include other aspects such as cytoplasmic viscosity, cortexillin-I dynamics, and membrane/cortex surface and curvature.

SUPPLEMENTAL REFERENCES

1. Robinson, D.N., Ocon, S.S., Rock, R.S., and Spudich, J.A. (2002). Dynacortin is a novel actin bundling protein that localizes to dynamic actin structures. J. Biol. Chem. *277*, 9088-9095.
2. Ruppel, K.M., Uyeda, T.Q.P., and Spudich, J.A. (1994). Role of highly conserved lysine 130 of myosin motor domain. In vivo and in vitro characterization of site specifically mutated myosin. J. Biol. Chem. *269*, 18773-18780.
3. Chen, P., Ostrow, B.D., Tafuri, S.R., and Chisholm, R.L. (1994). Targeted disruption of the *Dictyostelium* RMLC gene produces cells defective in cytokinesis and development. J. Cell Biol. *127*, 1933-1944.
4. Robinson, D.N., and Spudich, J.A. (2000). Dynacortin, a genetic link between equatorial contractility and global shape control discovered by library complementation of a Dictyostelium discoideum cytokinesis mutant. J. Cell Biol. *150*, 823-838.
5. Larochelle, D.A., Vithalani, K.K., and DeLozanne, A. (1996). A novel member of the *rho* family of small GTP-binding proteins is specifically required for cytokinesis. J. Cell Biol. *133*, 1321-1329.
6. Girard, K.D., Chaney, C., Delannoy, M., Kuo, S.C., and Robinson, D.N. (2004). Dynacortin contributes to cortical viscoelasticity and helps define the shape changes of cytokinesis. EMBO J. *23*, 1536-1546.
7. Octtaviani, E., Effler, J.C., and Robinson, D.N. (2006). Enlazin, a natural fusion of two classes of canonical cytoskeletal proteins, contributes to cytokinesis dynamics. Mol. Biol. Cell *17*, 5275-5286.
8. Reichl, E.M., Ren, Y., Morphew, M.K., Delannoy, M., Effler, J.C., Girard, K.D., Divi, S., Iglesias, P.A., Kuo, S.C., and Robinson, D.N. (2008). Interactions between myosin and actin crosslinkers control cytokinesis contractility dynamics and mechanics. Curr. Biol. *18*, 471-480.
9. Effler, J.C., Kee, Y.-S., Berk, J.M., Tran, M.N., Iglesias, P.A., and Robinson, D.N. (2006). Mitosis-specific mechanosensing and contractile protein redistribution control cell shape. Curr. Biol. *16*, 1962-1967.

10. Moores, S.L., Sabry, J.H., and Spudich, J.A. (1996). Myosin dynamics in live Dictyostelium cells. Proc. Natl. Acad. Sci. USA *93*, 443-446.
11. Sabry, J.H., Moores, S.L., Ryan, S., Zang, J.-H., and Spudich, J.A. (1997). Myosin heavy chain phosphorylation sites regulate myosin localization during cytokinesis in live cells. Mol. Biol. Cell *8*, 2647-2657.
12. Uyeda, T.Q., Abramson, P.D., and Spudich, J.A. (1996). The neck region of the myosin motor domain acts as a lever arm to generate movement. Proc. Natl. Acad. Sci. USA *93*, 4459-4464.
13. Zang, J.-H., and Spudich, J.A. (1998). Myosin II localization during cytokinesis occurs by a mechanism that does not require its motor domain. Proc. Natl. Acad. Sci. USA *95*, 13652-13657.
14. Hostetter, D., Rice, S., Dean, S., Altman, D., McMahon, P.M., Sutton, S., Tripathy, A., and Spudich, J.A. (2004). Dictyostelium myosin bipolar thick filament formation: importance of charge and specific domains of the myosin rod. PLoS Biol. *2*, e356.
15. Robinson, D.N., Cavet, G., Warrick, H.M., and Spudich, J.A. (2002). Quantitation of the distribution and flux of myosin-II during cytokinesis. BMC Cell Biology *3*, 4.
16. Zhang, W., and Robinson, D.N. (2005). Balance of actively generated contractile and resistive forces controls cytokinesis dynamics. Proc. Natl. Acad. Sci. USA *102*, 7186-7191.
17. Kovacs, M., Thirumurugan, K., Knight, P.J., and Sellers, J.R. (2007). Load-dependent mechanism of nonmuscle myosin 2. Proc. Natl. Acad. Sci. USA *104*, 9994-9999.
18. Veigel, C., Molloy, J.E., Schmitz, S., and Kendrick-Jones, J. (2003). Load-dependent kinetics of force production by smooth muscle myosin measured with optical tweezers. Nat. Cell Biol. *5*, 980-986.
19. Egelhoff, T.T., Lee, R.J., and Spudich, J.A. (1993). *Dictyostelium* myosin heavy chain phosphorylation sites regulate myosin filament assembly and localization *in vivo*. Cell *75*, 363-371.
20. Mahajan, R.K., and Pardee, J.D. (1996). Assembly mechanism of *Dictyostelium* myosin II: Regulation by K^+, Mg^{2+}, and actin filaments. Biochemistry *35*, 15504-15514.
21. Moores, S.L., and Spudich, J.A. (1998). Conditional Loss-of-Myosin-II-Function Mutants Reveal a Position in the Tail that Is Critical for Filament Nucleation. Mol. Cell *1*, 1043-1050.
22. Yumura, S., Yoshida, M., Betapudi, V., Licate, L.S., Iwadate, Y., Nagasaki, A., Uyeda, T.Q., and Egelhoff, T.T. (2005). Multiple myosin II heavy chain kinases: roles in filament assembly control and proper cytokinesis in Dictyostelium. Mol. Biol. Cell *16*, 4256-4266.
23. Davis, J.S. (1993). Myosin thick filaments and subunit exchange: A stochastic simulation based on the kinetics of assembly. Biochemistry *32*, 4035-4042.

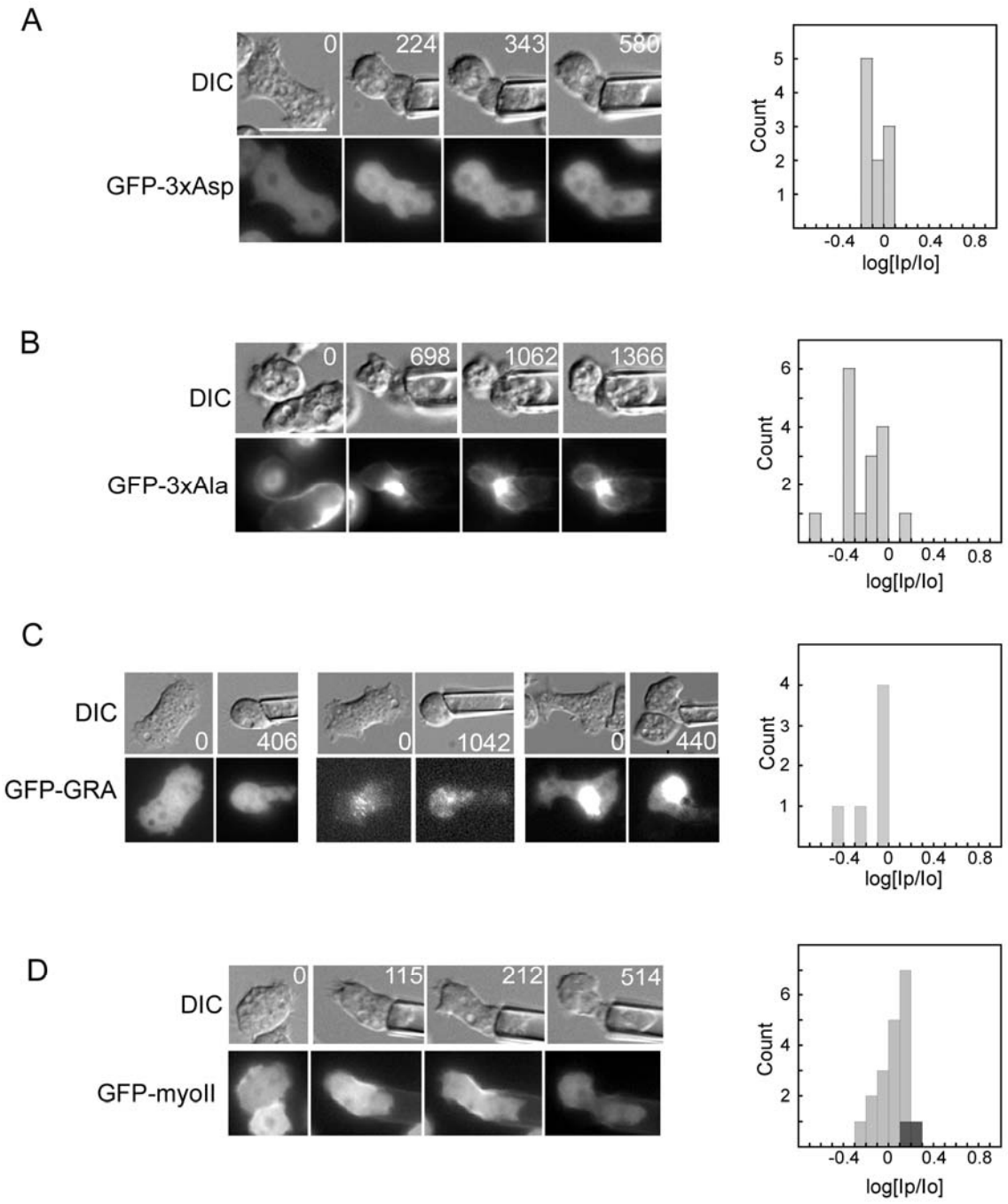

Figure S1. Wild type myosin-II assembly dynamics are required for the mechanosensory response. Time series (times in s) of DIC and fluorescence images are shown for (A) a *myoII*: GFP-3xAsp cell; (B) a *myoII*: GFP-3xAla cell; (C) three different *myoII:* GFP-RLCBS-AD (GRA) cells expressing varying amounts of GFP-GRA and aspirated using pressures of 0.39, 0.44 and 0.51 nN/μm^2, respectively, and (D) a *ΔRLC*: RLC(S13A);GFP-myoII. Frequency histograms show measurements from all cells measured for each genotype. As described in the Methods, the dark grey bars of the histograms indicate positive responses, while light grey bars indicate negative responses. Scale bar, 10 μm.

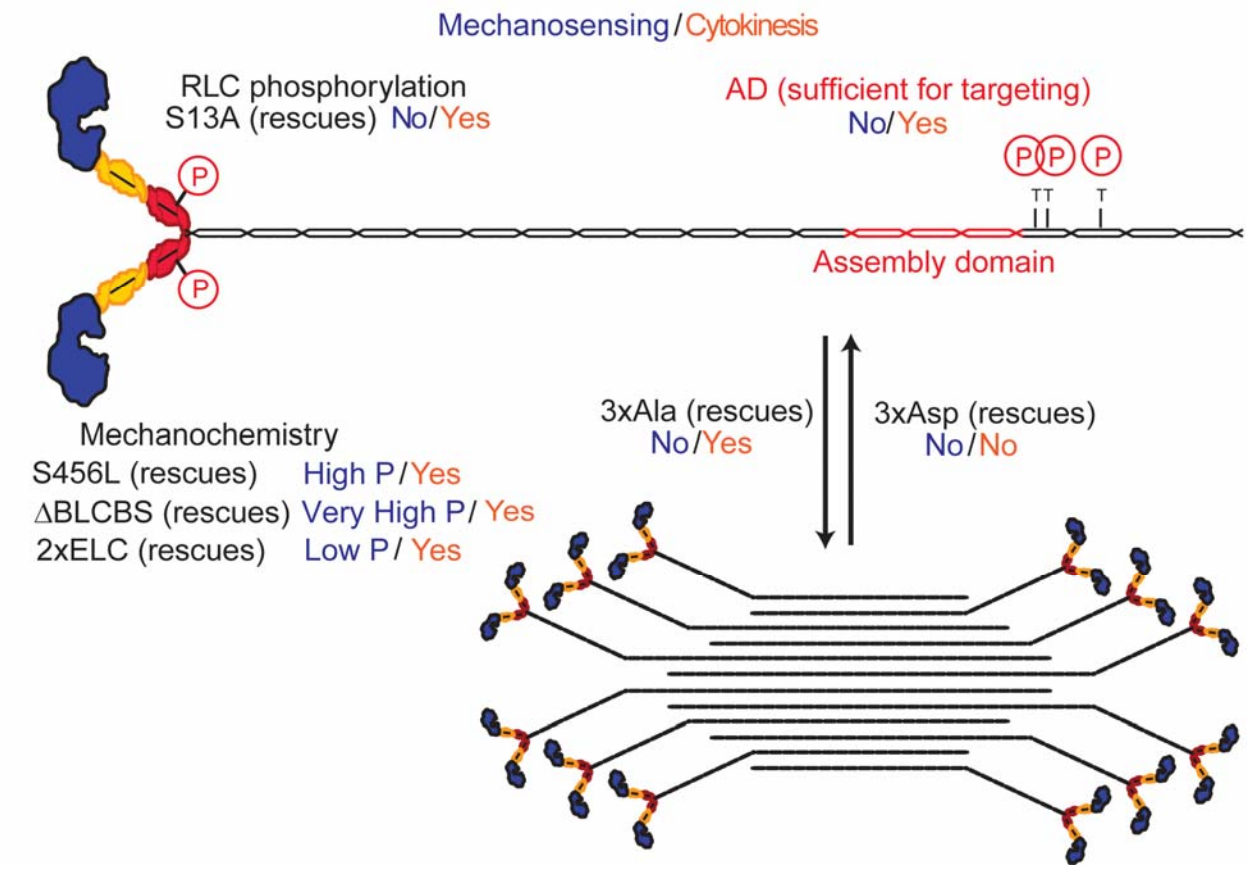

Figure S2. Summary of myosin-II mutants analyzed and a comparison of their requirements for mechanosensing vs. cytokinesis. Pressure, P.

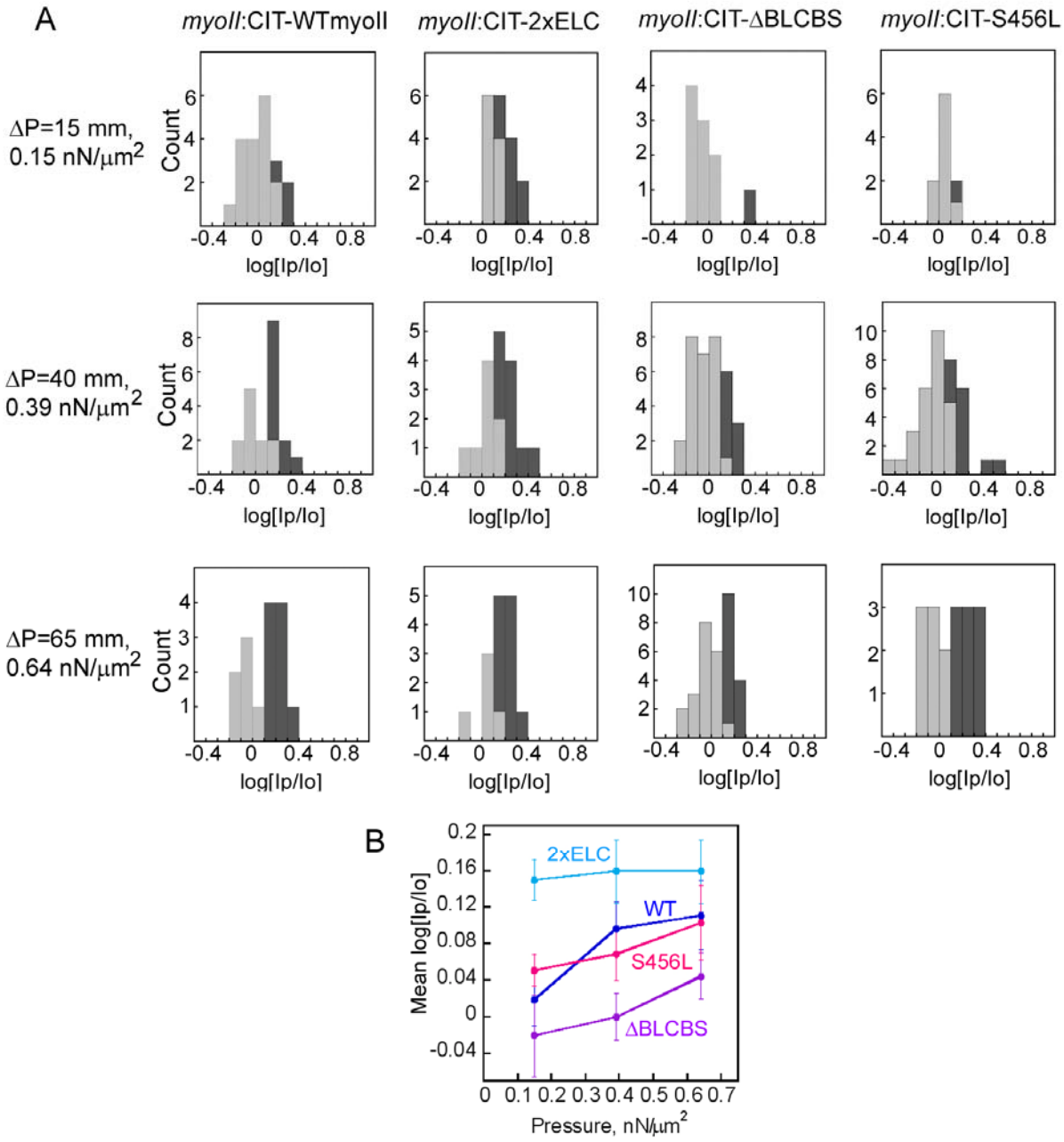

Figure S3. Frequency histograms showing the responses of wild type, ΔBLCBS, 2xELC and S456L myosin-II motors at the indicated pressures. These data in panel (A) are summarized in Fig. 1D in the main text. While the intensities are easily separated as responses and non-responses as described in the Methods, for an independent check we present the pressure dependency of the mean log[Ip/Io] (±SEM) values for the entire datasets (B). This approach considers all of the measurements without added assumptions and in this presentation, the data still fall into three classes according to lever arm length (2xELC, wild type and ΔBLCBS). Student's *t*-test results are included in Fig. 1 legend in the main text.

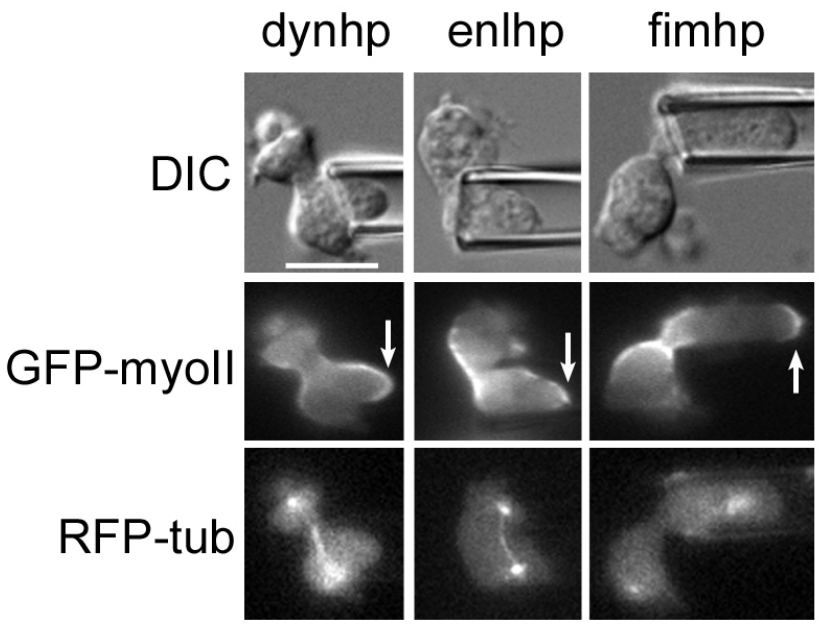

Figure S4. Actin crosslinkers dynacortin, fimbrin, and enlazin are not required for mechanosensing. Cells expressing GFP-myosin-II and RFP-tubulin had dynacortin, enlazin or fimbrin silenced by RNA interference (see Supplementary Methods). Arrows show the responses. Scale bar, 10 μm.

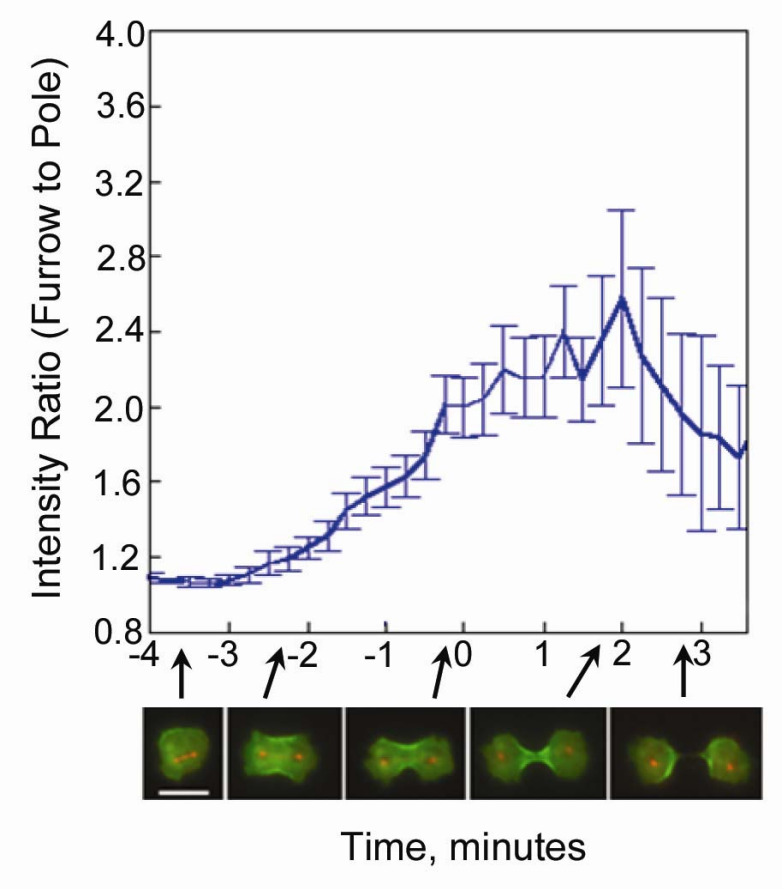

Figure S5. GFP-myosin-II distribution vs. time. Time is in minutes. D_x represents a distance of 2.7 μm, which was set to time 0 as described [16]. Ratio of average GFP-myosin-II intensity in the furrow cortex relative to the average intensity of the polar cortex was measured every 15 seconds (blue line). Two-color images reveal the mitotic spindle (RFP-tubulin) and GFP-myosin-II localization at each time-point. Data are based on n=10 cells; the curve is the average±SEM. The intensity ratios of 1.4-2 observed in the micropipette (Fig. S6) are comparable to the intensity ratios observed at the cleavage furrow cortex.

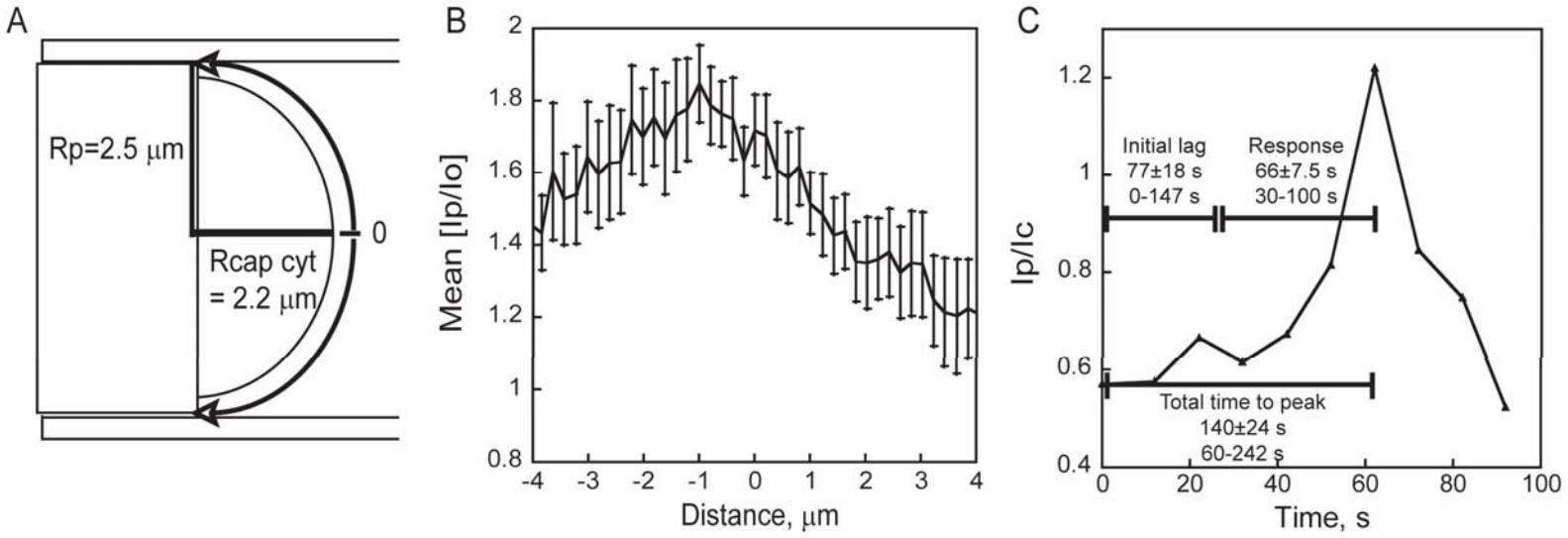

Figure S6. Dimensions of the hemispherical cap, radial myosin-II intensity and kinetics of myosin-II accumulation at the micropipette. (A) The geometry of the cortex in the micropipette. Here we assume the cortex is 0.35-μm thick comparable to other measurements. From this, the volume of the cytoplasm in the hemispherical cap is 22 μm^3, and the volume of the hemispherical cap cortex is 11 μm^3. The surface area of the hemisphere is 40 μm^2. (B) The circumferential line plot shows the Cit-wild type myosin-II signal intensity around the cortex measured for 9 responding cells. The 0 μm corresponds to the 0 point in panel A. The global average intensity ratio in the hemispherical cortex (from -4 to 4 μm) is 1.5±0.42 (mean±SD, n=410). (C) To detail the kinetics of the response, we analyzed the time required for the peak response to occur. Graph shows an example time-course. From the start of the movie, there is a lag time before any myosin-II accumulation is detectable, and the response time is the time required for the signal to rise from baseline to the peak. The total time is the time from the start of the experiment to the peak. For this kinetic analysis, we normalized the intensity in the pipette (Ip) to the local intensity of the cytoplasm (Ic). This region was more dependably in focus at each time point. As a result, the response ratio is a little lower than when normalizing to the opposite cortex (Io). The mean±SEM times and the range of the times are provided for each phase. The dataset is based on the same 9 cells as analyzed for panel B.

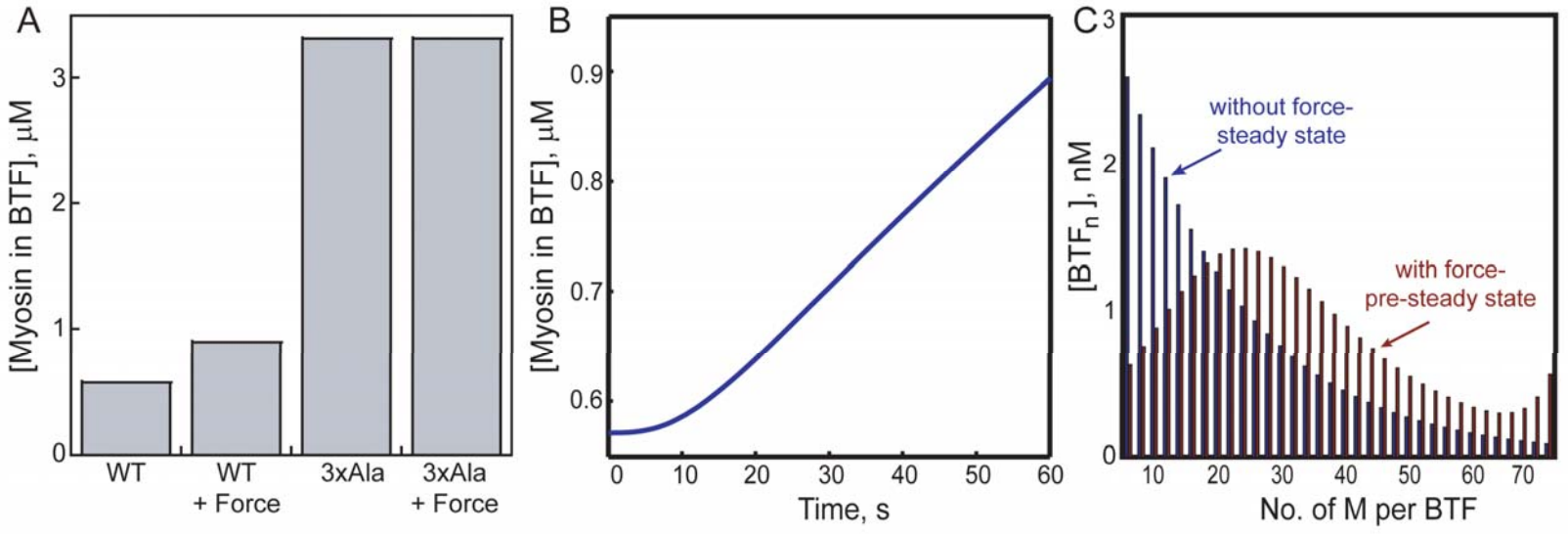

Figure S7. Simulation and sensitivity analysis reveals a potential force-sensitive step in myosin-II bipolar thick filament assembly. (A) Graph shows that a 10-fold change in k_1 yields a 50% increase in assembled myosin-II. 3xAla is already nearly completely assembled, preventing further force-sensitive assembly. (B) Graph shows that force-induced assembly occurs on the minute time-scale. Time 0 shows the initial steady state before k_{-1} is shifted down 10-fold (to mimic the impact of force). By 60 s, the concentration of myosin in BTF form is increased 1.5-fold, similar to that observed in the micropipette. (C) Graph shows the distribution of BTF sizes before (without force – steady state) and 60 s after (with force – pre-steady state) the 10-fold change in k_{-1}. Shifting k_{-1} increases the average size of the BTFs.

Table S1. *Dictyostelium* strains used in this study

Strain	Genotype	Question	# Responses/ Total Cells
myoII:: RFP-α-tubulin; GFP-myoII; pLD1	*myoII*(HS1)::RFP-α-tubulin,Bl^{R}:pDXA-Bl; GFP-myoII, Hyg^{R}: pDRH; pLD1,G418^{R}: pLD1A15SN	Influence of crosslinkers on mechanosensory response	1/4
myoII:: RFP-α-tubulin; GFP-myoII; dynhp	*myoII*(HS1)::RFP-α-tubulin,Bl^{R}:pDXA-Bl; GFP-myoII, Hyg^{R}: pDRH; dynhp,G418^{R}: pLD1A15SN		2/4
myoII:: RFP-α-tubulin; GFP-myoII;fimhp	*myoII*(HS1)::RFP-α-tubulin,Bl^{R}:pDXA-Bl; GFP-myoII, Hyg^{R}: pDRH; fimhp,G418^{R}: pLD1A15SN		6/13
myoII:: RFP-α-tubulin; GFP-myoII; enlhp	*myoII*(HS1)::RFP-α-tubulin,Bl^{R}:pDXA-Bl; GFP-myoII, Hyg^{R}: pDRH; enlhp,G418^{R}: pLD1A15SN		4/7
myoII::GFP-cortI	*myoII*(HS1)::GFP-cortI,Hyg^{R}:pDRH; G418^{R}:pLD1A15SN	Cortexillin-I dependency on myosin-II	0/15
myoII:: GFP-cortI; dynhp	*myoII*(HS1)::GFP-cortI,Hyg^{R}:pDRH; dynhp,G418^{R}:pLD1A15SN		0/13
myoII:: GFP-cortI; S456L	*myoII*(HS1)::GFP-cortI,Hyg^{R}:pDRH; S456L,G418^{R}:pBIG		1/13
myoII:: GFP-cortI; myoII	*myoII*(HS1)::GFP-cortI,Hyg^{R}:pDRH; myoII, G418^{R}:pBIG		14/32
KAx3:: GFP-myoII; RFP-α-tubulin	KAx3::RFP-α-tubulin, Hyg^{R}:pDRH; GFP-myoII, G418^{R}: pBIG	Wild type parent of *cortI*(RF) strain	6/7
cortI:: GFP-myoII; RFP-α-tubulin	*cortI*(RF)::RFP-α-tubulin, Hyg^{R}:pDRH; GFP-myoII, G418^{R}: pBIG	Myosin-II dependency on cortexillin-I	0/10
cortI:: GFP-myoII; RFP-ΔNcortI	*cortI(RF)::* RFP-ΔNcortI, Hyg^{R}:pDRH; GFP-myoII, G418^{R}: pBIG		6/19
cortI:: GFP-myoII; RFP-cortI	*cortI(RF)::* RFP-cortI, Hyg^{R}:pDRH; GFP-myoII, G418^{R}: pBIG		7/10
cortI^{1151}:: GFP-myoII; RFP-α-tubulin	*cortI*^{1151}::RFP-α-tubulin,Hyg^{R}:pDRH;GFP-myoII, G418^{R}: pBIG		0/15
cortI^{1151}:: GFP-myoII; RFP-cortICT	*cortI*^{1151}:: RFP-cortICT,Hyg^{R}:pDRH; GFP-myoII,G418^{R}: pBIG		1/13
cortI^{1151}:: GFP-myoII; RFP-cortI	*cortI*^{1151}:: RFP- cortI,Hyg^{R}:pDRH; GFP-myoII,G418^{R}: pBIG		5/8

Strain	Genotype	Question	# Responses/ Total Cells
myoII: RFP-α-tubulin; GFP-myoII	*myoII*(HS1)::GFP-myoII, G418^{R}:pBIG; RFP-α-tubulin, Hyg^{R}: pDRH	Assembly dynamics (wild type control)	16/26*
myoII: RFP-α-tubulin; GFP-GRA	*myoII*(HS1)::GFP-RLCBS-Assembly Domain; RFP-α-tubulin, Hyg^{R}: pDRH	Sufficiency of minimal cleavage furrow targeting domain	0/6
myoII: RFP-α-tubulin; GFP-3xAsp	*myoII*(HS1)::GFP-3xAsp myoII, G418^{R}:pBIG; RFP-α-tubulin, Hyg^{R}:pDRH	Myosin assembly dynamics	0/10
myoII: RFP-α-tubulin; GFP-3xAla	*myoII*(HS1)::GFP-3xAla myoII, G418^{R}:pBIG; RFP-α-tubulin, Hyg^{R}:pDRH	Myosin disassembly dynamics	0/16
ΔRLC: RLC-S13A; GFP-myoII	*ΔRLC:* RLC-S13A, G418^{R}; GFP-myoII, Hyg^{R}: pDRH	Role of myosin RLC phosphorylation	2/19
ΔRLC: RLC; GFP-myoII	*ΔRLC:* RLC (wt), G418^{R}; GFP-myoII, Hyg^{R}: pDRH		7/11
myoII: GFP-α-tubulin; Citrine-myoII	*myoII*(HS1)::Cit-myoII, Hyg^{R}:pDRH; GFP-α-tubulin, G418^{R}:pDEX	Role of myosin-II mechanochemistry and wild type 9-nm lever arm (wild type control)	ΔP15 mm – 3/20 ΔP40 mm – 10/21 ΔP65 mm – 9/15
myoII: GFP-α-tubulin; Citrine-S456L myoII	*myoII*(HS1)::Cit-myoII (S456L), Hyg^{R}:pDRH; GFP-α-tubulin, G418^{R}:pDEX	Role of myosin-II mechanochemistry	ΔP15 mm – 1/10 ΔP40 mm – 11/37 ΔP65 mm – 9/17
myoII: GFP-α-tubulin; Citrine-ΔBLCBS myoII	*myoII*(HS1)::Cit-myoII (ΔBLCBS), Hyg^{R}:pDRH; GFP-α-tubulin, G418^{R}:pDEX	2-nm long lever arm	ΔP15 mm – 1/10 ΔP40 mm – 8/34 ΔP65 mm – 13/33
myoII: GFP-α-tubulin; Citrine-2xELC myoII	*myoII*(HS1)::Cit-myoII (2xELC), Hyg^{R}:pDRH; GFP-α-tubulin, G418^{R}:pDEX	13-nm long lever arm	ΔP15 mm – 8/18 ΔP40 mm – 9/17 ΔP65 mm – 10/15
RacE: GFP-myoII; RFP-α-tubulin	*RacE^{24EH6}::*GFP-myoII G418^{R}:pBIG; RFP-α-tubulin, Hyg^{R}:pDRH	RacE inhibition of mechanosensory response	Mitotic – 2/5 Interphase – 23/37
RacE: GFP-myoII; mCherry-RacE	*RacE^{24EH6}::*GFP-myoII G418^{R}:pBIG; mCherry-RacE, Hyg^{R}, pDRH		Interphase – 2/20
RacE: GFP-cortI	*RacE^{24EH6}::*GFP-cortI; G418^{R}: pEXP4		Interphase – 15/37

*Sup. Ref [9].